Nacre-Inspired Design of Mechanical Stable Coating with Underwater Superoleophobicity

Li-Ping Xu,[†] Jitao Peng,[†] Yibiao Liu,[†] Yongqiang Wen,[†] Xueji Zhang,[†] Lei Jiang,[‡] and Shutao Wang[‡,*]

[†]Research Center for Bioengineering and Sensing Technology, University of Science & Technology Beijing, Beijing 100083, P.R. China and [‡]Beijing National Laboratory for Molecular Sciences (BNLMS), Key Laboratory of Organic Solids, Institute of Chemistry, Chinese Academy of Sciences, Beijing 100190, P.R. China

ABSTRACT Because of the frequent oil spill accidents in marine environment, stable superoleophobic coatings under seawater are highly desired. Current underwater superoleophobic surfaces often suffer from mechanical damages and lose their superoleophobicity gradually. It remains a challenge to fabricate a stable and robust underwater superoleophobic film which can endure harsh conditions in practical application. Nacre is one of most extensively studied rigid biological materials. Inspired by the outstanding mechanical property of seashell nacre and those underwater superoleophobic surfaces from nature, we fabricated a polyelectrolyte/clay hybrid film *via* typical layer-by-layer (LBL) method based on building blocks with high surface energy. `Bricks-and-mortar' structure of seashell nacre was conceptually replicated into the prepared film, which endows the obtained film with excellent mechanical property and great abrasion resistance. In addtion, the prepared film also exhibits stable underwater superoleophobicity, low oil adhesion, and outstanding environment durability in artificial seawater. We anticipate that this work will provide a new method to design underwater low-oil-adhesion film with excellent mechanical property and improved stability, which may advance the practical applications in marine antifouling and microfluidic devices.

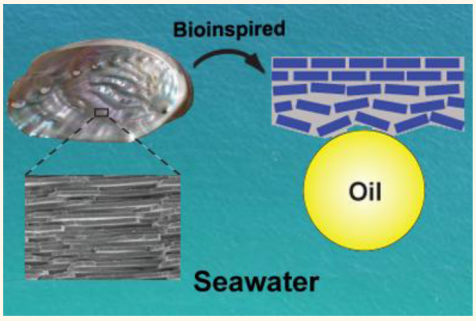

KEYWORDS: underwater · nacre · superoleophobicity · oil-adhesion · layer-by-layer · interfaces

Superoleophobic coatings have been emerging as one hot topic in the field of fundamental surface science[1−8] and practical coating applications.[9−19] Due to the high frequency of oil spill accidents in marine environment, underwater superoleophobic coating is in urgent demand. However, the presence of water nullifies the oil repellency capability of traditional fluorinated superoleophobic coatings.[20−23] Recently, the discovery of unique underwater−oil-repellent property of fish scale and clam shell brought a new way to overcome this predicament by introducing high-energy materials, including polymer hydrogel coatings[24−27] and copper oxide coating.[2,28] Those studies revealed that the combination of hierarchical micro/nanostructures and surface with high surface energy is generally required for obtaining underwater superoleophobicity. However, most of those underwater superoleophobic films based on hydrogel[25] are prone to collapse and deformation due to their typically weak stiffness and strength of hydrogels, and can not keep their superoleophobicity. The detachment of some underwater superoleophobic film may also be observed.[29] Moreover, those surfaces often suffer from mechanical damage, such as fluid flush in seawater and inevitable scraping/rubbing. Their poor mechanical properties result in a gradual loss of superoleophobicity. Underwater superoleophobic coatings need to endure harsh conditions in practical application.[30] But it remains a challenge to fabricate a stable and robust underwater superoleophobic film.

Nature has evolved materials that exhibit exceptionally excellent mechanical properties. Among those few well-known examples including bones, teeth, nacres, *etc.*, nacre is one of the most extensively studied biological models. In aiming to develop analogous man-made materials, several studies were carried out by investigating and modeling their architectures and compositions from micro- to nanoscale. The excellent mechanical properties of seashell nacres originate from the layered arrangement of

* Address correspondence to stwang@iccas.ac.cn.

Received for review February 6, 2013 and accepted May 17, 2013.

Published online May 17, 2013
10.1021/nn400650f

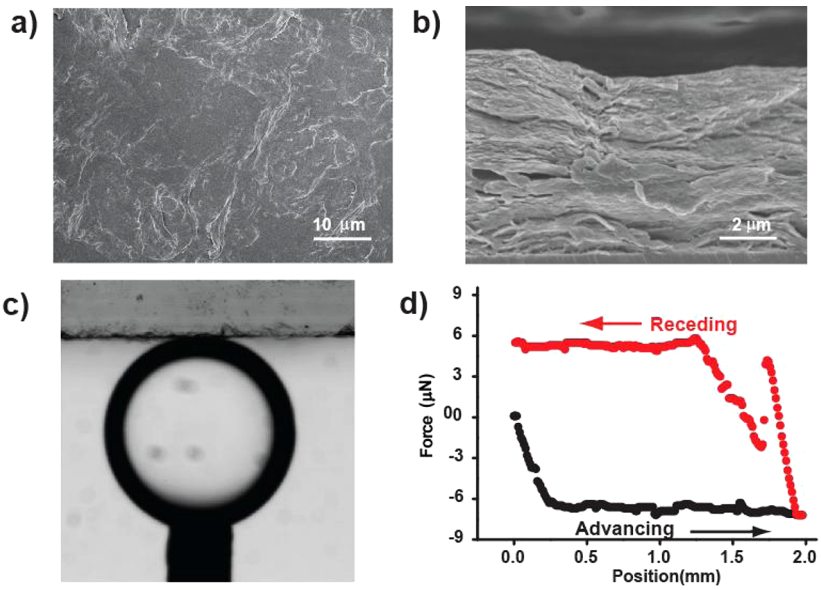

Figure 1. The SEM images and wettability measurements on $(MTM/PDDA)_{100\text{-}salt}$ film. (a) top-view and (b) cross section SEM image of $(MTM/PDDA)_{100\text{-}salt}$ film; (c) photograph of *n*-decane oil droplet at the water/$(MTM/PDDA)_{100\text{-}salt}$ interface; (d) the measurement of underwater−oil adhesion on $(MTM/PDDA)_{100\text{-}salt}$ film. The detected force is 3.4 ± 1.1 μN. Detecting probe is *n*-decane oil droplet.

inorganic nanoplatelets and proteins into a "bricks-and-mortar" nanostructure.[31−41] This unique layered nanostructure of nacre may give scientists some enlightenment in fabricating novel functional materials with excellent mechanical properties. Kotov's group has fabricated a series of nacre-like artificial films through layer-by-layer assembly using clays and polymers as building blocks.[32,42,43] Yu *et al.* fabricated artificial nacre-like chitosan-montmorillonite clay (MTM) bionanocomposite films with high performance in mechanical, light transmittance, and fire resistant properties.[35] Nacre-like responsive films were fabricated with poly(*N*-isopropylacrylamide) (PNIPAM) and MTM nanoplatelets and these films also exhibit strong mechanical properties. Those recent advances in nacre-inspired rigid materials showed the great success in fabricating artificial materials with excellent mechanical performance.[44,45] However, nacre-inspired film with underwater superoleophobicity has not been reported in previous work.

In this work, inspired by nacre's excellent mechanical properties and those underwater superoleophobic surfaces from nature, we design and fabricate a layered coating with robust and stable underwater superoleophobicity *via* layer-by-layer (LBL) assembly. LBL assembly is a versatile method which can construct nanoscale films, surfaces, and functional materials with highly tunable architectures and properties.[29,46−49] Since MTM and polyelectrolytes (including poly(4-styrenesulfonic acid) (PSS) and poly(diallyldimethylammonium chloride) (PDDA)) are high-energy materials, which are suitable for making underwater superoleophobic film, MTM nanoplatelets were selected as ideal inorganic building blocks and polyelectrolytes were employed as organic matrixes to fabricate "bricks-and-mortar" structures. For fabricating robust film with stable underwater superoleophobicity in seawater, the LBL process was performed in 0.5 M NaCl since 0.5 M NaCl is very close to seawater salinity.[29] Because of the nacre-like microstructure, ion-induced roughness increment and high surface energy of employed building blocks, the obtained $(MTM/PDDA)_{100\text{-}salt}$ film not only displays excellent mechanical properties, but also possesses stable superoleophobicity under seawater.

RESULTS AND DISCUSSION

Scanning electron microscopy (SEM) image of $(MTM/PDDA)_{100\text{-}salt}$ film (Figure 1a) confirmed dense coverage and planar orientation of the MTM nanoplatelets. Wrinkle structure was also observed. Cross-section SEM image of the $(MTM/PDDA)_{100\text{-}salt}$ film (Figure 1b) revealed a well-defined layered structure which was conceptually similar to that of nacre. Each layer appears wavelike structure. Tapping mode AFM image (Figure S4b) indicated that several bumps and depressions were observed and the roughness of $(MTM/PDDA)_{100\text{-}salt}$ film is 709.9 nm. The thickness of the film cross sections was 4.7 ± 0.3 μm. This value is higher than that reported in previous paper (a 200 bilayer film of PDDA/C has a thickness of *ca.* 4.9 μm),[38] which might result from the different ion-strength of assembly solution and different measuring angle between cross section and substrate.

Underwater−oil wettability of $(MTM/PDDA)_{100\text{-}salt}$ film was characterized with a contact-angle instrument by using an oil droplet (*n*-decane) as a detecting probe. $(MTM/PDDA)_{100\text{-}salt}$ film was placed in distilled water. After that, the *n*-decane oil droplet (2 μL) was syringed out and

dropped carefully onto the film. $(MTM/PDDA)_{100\text{-salt}}$ film exhibits superoleophobicity with an oil contact angle (OCA) of $164.5 \pm 0.4°$ (Figure 1c). The *n*-decane droplet on $(MTM/PDDA)_{100\text{-salt}}$ film appeared as a round ball. A high sensitivity micro electromechanical balance system was utilized to measure the oil-adhesion forces quantitatively (Figure 1d). During the whole measurement, the detected adhesive force is 3.4 ± 1.1 μN. The oil droplet on $(MTM/PDDA)_{100\text{-salt}}$ film could be transferred away without residual left. These results demonstrate that the $(MTM/PDDA)_{100\text{-salt}}$ film is superoleophobic underwater with low oil adhesion.

Other oils with different surface tensions including 1, 2-dichloroethane, trichloromethane, *n*-hexane, petroleum ether and crude oil were also employed as detecting probe in OCA and oil-adhesion force measurements (Table 1). The comparison results show that $(MTM/PDDA)_{100\text{-salt}}$ film exhibits underwater superoleophobicity and low adhesive forces to all utilized oil. We also prepared $(MTM/PDDA)_{100\text{-salt}}$ film with MTM layer exposed. The OCA on $(MTM/PDDA)_{100\text{-salt}}$ is $163.3 \pm 2.1°$ with *n*-decane as indicating probe, and the underwater adhesive force between *n*-decane droplet and $(MTM/PDDA)_{100\text{-salt}}$ film is 4.2 ± 0.5 μN. The results indicate that $(MTM/PDDA)_{100\text{-salt}}$ film is superoleophobic underwater with low oil-adhesion no matter which layer is exposed outside.

TABLE 1. The Underwater Oil Contact Angles and Adhesive Forces between $(MTM/PDDA)_{100\text{-salt}}$ Film and Oil with Different Surface Tension Values

oil	surface tension @25 °C (mN/m)[a]	contact angle (deg)	adhesive force (μN)
1, 2-Dichloroethane	31.86[1]	168.7 ± 2.5	0
Trichloromethane	26.67[1]	163.5 ± 1.5	1.3 ± 1.2
Crude Oil	27.44—34.64 (20 °C)[2]	166.5 ± 1.2	1.8 ± 1.9
n-Decane	23.37[1]	164.5 ± 0.4	3.4 ± 1.1
n-Hexane	18.40[1]	160.9 ± 0.9	4.0 ± 1.9
Petroleum Ether	17.5 (15 °C)[3]	162.1 ± 1.0	4.7 ± 2.7

[a] Surface tension values of different test oils were obtained from: (1) ref [50], (2) ref [51], (3) ref [52].

The mechanical properties of $(MTM/PDDA)_{100\text{-salt}}$ multilayers were characterized by nanoindentation experiments. Typical indent profile and force-displacement curve of $(MTM/PDDA)_{100\text{-salt}}$ multilayers are shown in Figure 2a,b. According to the AFM image of the indented region of $(MTM/PDDA)_{100\text{-salt}}$ film upon removal of maximum loads of 5000 μN, residual deformation was clearly visible, exhibiting a central indent and a pileup zone indicating plastic flow of the material from beneath the indenter. No microcracks were evident with the residual indent region, in the pileup zone, or in the area immediately outside the residual indent. Young's modulus is an important parameters to evaluate the mechanical performance of the materials, which could be obtained from nanoindentation experiments.[53] Young's modulus of $(MTM/PDDA)_{100\text{-salt}}$ film is 9.4 ± 2.4 GPa, which is in the same order of magnitude of the Young's modulus of nature nacre. Compared with LBL films made only from polyelectrolytes, Young's modulus is increased

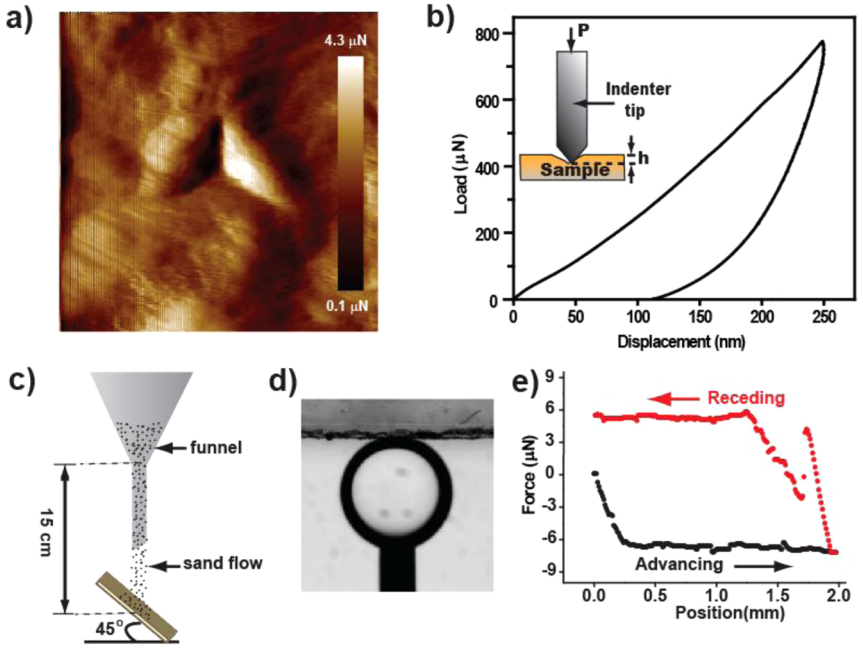

Figure 2. Mechanical properties of $(MTM/PDDA)_{100\text{-salt}}$ film. (a) AFM image of residual nanoindentation impression on $(MTM/PDDA)_{100\text{-salt}}$ film, the maximum load is 5000 μN, image size: 10 μm × 10 μm; (b) load—displacement data for artificial nacre $(MTM/PDDA)_{100\text{-salt}}$ film; (c) Scheme of a sand abrasion experiment; (d) contact angle of *n*-decane oil droplet at the water/$(MTM/PDDA)_{100\text{-salt}}$ film after 5 g of sand abrasion from 15 cm height; (e) underwater—oil adhesive force measurement on $(MTM/PDDA)_{100\text{-salt}}$ film after sand abrasion from 15 cm height. Detecting probe is *n*-decane oil droplet.

significantly from 0.7−1 GPa[54,55] to around 10 GPa. $(MTM/PDDA)_{100\text{-salt}}$ film is composed of `soft' polyelectrolyte mortar and `hard' clay bricks. As shown in Figure S1, `hard' clay bricks were observed to adsorb in the form of a densely packed layer with parallel orientation to the substrate. The polymer chains can be arranged in coils and folds, physically pinned by electrostatic interactions. As the film is deformed and the clay nanoplatelets begin to slide over each other, and molecular rearrangements happens with the concomitant unfolding of coiled polymer chains. The `brick-and-mortar' structure endows the film with Young's modulus that approaches those of seashell nacre.[32,56]

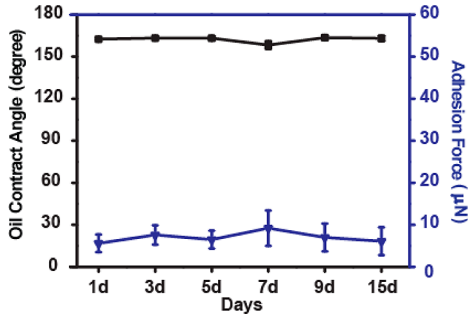

Figure 3. Durability of the superoleophobic coating. Contact angle (■) and adhesive force (▼) for an *n*-decane droplet at the water/$(MTM/PDDA)_{100\text{-salt}}$ interface after immersed in artificial seawater for several days. $(MTM/PDDA)_{100\text{-salt}}$ film keeps its oil-repellent properties with the OCAs varying from 158.3° to 163.6° and the recorded maximum adhesion force is 9.2 μN. The surface exhibits superoleophobicity and low oil adhesion even after being exposed to artificial seawater for half month. Detecting probe is *n*-decane.

With the use of a sand abrasion test as a measure of harsh conditions, we verify the abrasion resistance of $(MTM/PDDA)_{100\text{-salt}}$ film. Sand grains with diameter of 150−300 μm impinged the surface from a height of 15 cm (Figure 2c). After sand abrasion, the underwater−oil wettability of this film was recharacterized. As shown in Figure 2d, the *n*-decane droplet kept spherical on $(MTM/PDDA)_{100\text{-salt}}$ film after sand impingement. $(MTM/PDDA)_{100\text{-salt}}$ film retained its underwater superoleophobicity with OCA of 161.9 ± 1.5°. Underwater−oil adhesive force measurement indicates

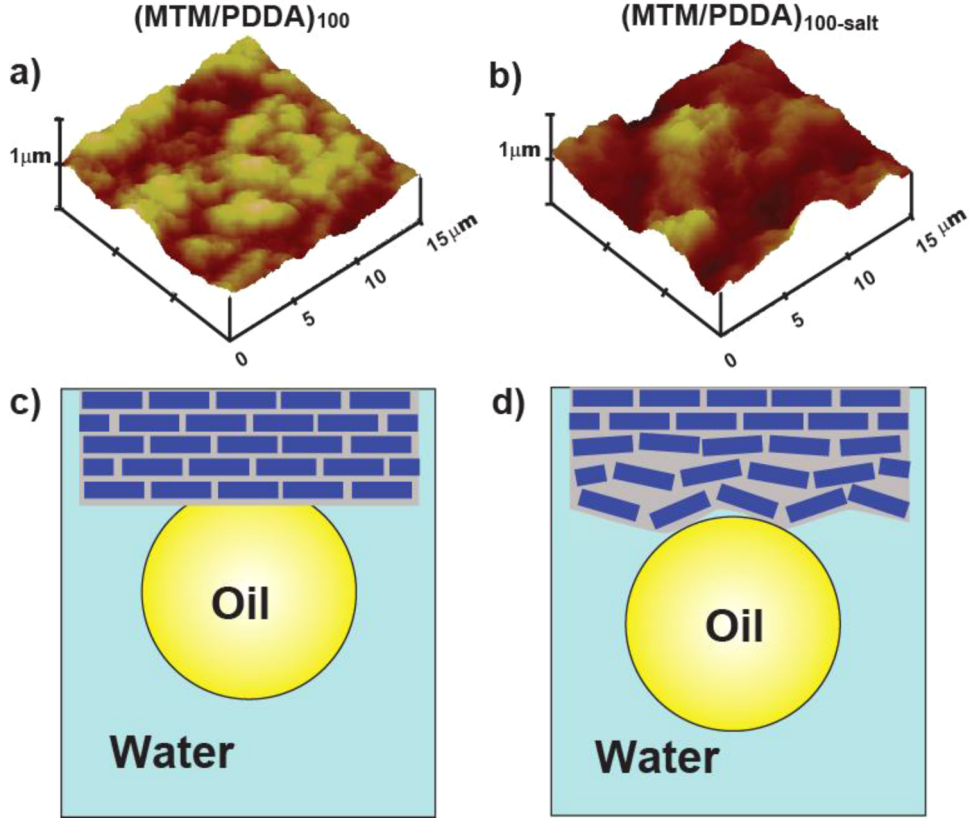

Figure 4. Effect of salt on surface structure and oil adhesion behavior of prepared films. (a and b) AFM images of $(MTM/PDDA)_{100}$ and $(MTM/PDDA)_{100\text{-salt}}$ film, respectively. AFM images showed the $(MTM/PDDA)_{100\text{-salt}}$ film is rougher with obvious bumps and depressions after introducing ions into polyelectrolyte solutions before LBL assembly, which can be ascribed to the coiling structure of the polyelectrolyte chains adsorbed at the surface in the present of 0.5 M NaCl, (c and d) Schematic mechanism for oil droplet wetting state on the $(MTM/PDDA)_{100}$ and $(MTM/PDDA)_{100\text{-salt}}$ film, respectively. Due to the low roughness of $(MTM/PDDA)_{100}$ film, oil droplet is in direct contact with solid film resulting in high oil-adhesion. For $(MTM/PDDA)_{100\text{-salt}}$ film with higher roughness, the contact line between oil droplet and solid film is discrete and water molecules were trapped between oil/solid interface, resulting in low oil-adhesion (the Cassie's state in water/oil/solid interface is obtained).

that impinged $(MTM/PDDA)_{100\text{-salt}}$ film has low adhesive force of 4.8 ± 1.4 μN to *n*-decane droplet (Figure 2e). Therefore, $(MTM/PDDA)_{100\text{-salt}}$ film is not vulnerable to falling sand, and keeps its underwater superoleophobicity and low-oil-adhesion after sand abrasion.

The durability in marine environment of $(MTM/PDDA)_{100\text{-salt}}$ film was also studied for assessing its potential as marine coating. A mixture of dissolved mineral salts was prepared to simulate seawater.[29] Underwater−oil wettability of $(MTM/PDDA)_{100\text{-salt}}$ film was rechecked after being exposed to artificial seawater for several days. As shown in Figure 3, $(MTM/PDDA)_{100\text{-salt}}$ film keeps its oil-repellent properties with the OCAs varying from 158.3° to 163.6° using *n*-decane as detecting probe. The oil-adhesive force of $(MTM/PDDA)_{100\text{-salt}}$ film was also investigated after exposing to artificial seawater. The recorded adhesion force between *n*-decane droplet and $(MTM/PDDA)_{100\text{-salt}}$ film is 5.6−9.2 μN. The surface exhibits low adhesion to the *n*-decane droplet and the *n*-decane droplet on film can always be drawn without loss. The results suggest that the underwater superoleophobic surface is stable, which originates from the good chemical and structural stability of polyelectrolyte/clay LBL film in seawater.

To understand the mechanism of the excellent stability of $(MTM/PDDA)_{100\text{-salt}}$ film in artificial seawater with high ion-strength, we studied the ion-effect on underwater oleophobicity. For comparison, another polyelectrolyte/clay hybrid film (abbreviated as $(MTM/PDDA)_{100}$ film) was prepared without adding NaCl in polyelectrolyte solution. According to OCA measurement, $(MTM/PDDA)_{100}$ film is oleophobic with *n*-decane CA of 131.0 ± 3.8° (Figure S3a). Adhesive force measurement indicates that $(MTM/PDDA)_{100}$ film exhibits high adhesion with *n*-decane droplet and the measured underwater adhesive force of 48.0 ± 5.6 μN (Figure S3b). Other oil droplets with different surface tension were also used to evaluate the underwater−oil wettability of $(MTM/PDDA)_{100}$ film (see Table S1) and results indicate that $(MTM/PDDA)_{100}$ film is high adhesive to all employed oil. AFM results (Figure 4a,b and Figure S4) indicate that $(MTM/PDDA)_{100\text{-salt}}$ film is rougher than $(MTM/PDDA)_{100}$ film due to the coiling of polyelectrolyte chains.[29,57−59] The surface RMS roughness of $(MTM/PDDA)_{100}$ and $(MTM/PDDA)_{100\text{-salt}}$ film is 99.4 and 144.8 nm, respectively. When an oil droplet is placed on $(MTM/PDDA)_{100}$ film under water, a continuous contact line is formed between oil droplet and $(MTM/PDDA)_{100}$ film (Figure 4c), which makes a Wenzel state with high oil adhesion. In contrast, water is trapped between oil droplet and $(MTM/PDDA)_{100\text{-salt}}$ film, which results in a typical Cassie's state with lower oil adhesion (Figure 4d). When $(MTM/PDDA)_{100\text{-salt}}$ was immersed in seawater, the high ion-strength of seawater favors the low underwater−oil-adhesion state. It thus endows $(MTM/PDDA)_{100\text{-salt}}$ film with stable superoleophobicity and low oil-adhesion in seawater.

CONCLUSIONS

In conclusion, inspired by the fascinating mechanical property of nacre and those underwater superoleophobic surfaces from nature, we demonstrated a new strategy for fabricating superoleophobic coating. "Bricks-and-mortar" nanostructure of seashell nacre was conceptually replicated and the prepared film shows good performance in underwater superoleophobicity, low oil adhesion, mechanical property, abrasion-resistance and environment durability in artificial seawater. This study provides a novel route to design underwater low-oil-adhesion film with excellent mechanical property and improved stability, which may boost practical applications in marine antifouling and microfluidic devices.

MATERIALS AND METHODS

Layer-by-Layer Assembly. Prior to film deposition, glass slides were cleaned by immersion in piranha solution (3:1 H_2SO_4:H_2O_2) for 5 min followed by thorough rinsing with distilled water. Subsequently, the glass slides were immersed in an ethanol solution of (3-aminopropy) triethoxysilane (1% volume ratio) for 12 h. Then, the positive charged substrate was alternatively immersed in an aqueous solution of PSS (1 mg/mL) and PDDA (1 mg/mL) for 10 min. This process was repeated four times to produce the $(PSS/PDDA)_4$ film. Finally, the $(PSS/PDDA)_4$ film was alternatively immersed in MTM clay suspension (0.5 wt %) for 5 min and PDDA solution (1 mg/mL, with 0.5 M NaCl) for 10 min. The process was repeated 100 times. Every deposition is followed by rinsing with distilled water for 2 min and drying with a stream of N_2 for 1 min. The LBL fabrication of $(MTM/PDDA)_{100\text{-salt}}$ film was performed under the condition of 0.5 M NaCl since 0.5 M NaCl is very close to seawater salinity and promotes the formation of high roughness surface.[29] Meanwhile, $(MTM/PDDA)_{100}$ film was fabricated in the absence of 0.5 M NaCl with keeping other experimental parameter unchanged.

During the adsorption step, MTM nanoplatelets become oriented parallel to the surface maximizing the attractive energy as imaged by AFM (Figure S1). The film is stabilized *via* strong attractive electrostatic and van der Waals interactions between polyelectrolytes and MTM nanoplatelets. The fabricating process of $(MTM/PDDA)_{100\text{-salt}}$ film was monitored by a Shimadzu UV-1800 spectrophotometer (Figure S2a) .

Instruments and Characterization. A field-emission scanning electron microscope (JSM-6700F, Japan) was used for characterizing the morphologies of the as-prepared film. AFM images were acquired under water with a Multimode 3D SPM instrument (Bruker) in the tapping mode. The resulting images were flattened and plane-fitted using software from Bruker. X-ray photoelectron spectroscopy (XPS) data were obtained with an ESCALab220i-XL electron spectrometer (VG Scientific) using 300W Al Kα radiation. The base pressure was about 3×10^{-9} mbar. Nanoindentation tests were performed using a Triboscope nanomechanical testing system (TI950, Hysitron, Inc.). The Hysitron nanoindenter monitors and records the load and displacement of the indenter, a diamond Berkovich three-sided pyramid.

Oil contact angles (OCA) were measured on an OCA20 system (Data-Physics, Germany) at ambient temperature. The oil droplet (*n*-decane or other oil, 2 μL) was syringed out and dropped carefully onto the surfaces, which were immersed in distilled water. The average OCA values were obtained by measuring at five different positions on the same sample. The adhesive forces were measured on a high-sensitivity microelectromechanical balance system (DCAT 11 system, Data-Physics, Germany). Typically, an oil drop (about 6 μL) was hung on a copper cap connected to the microbalance, and then the substrate was controlled to move toward the oil droplet at a constant speed of 0.05 mm s^{-1}, until it made contact with the oil droplet, at which point the substrate was then moved in reverse direction and left the oil droplet. During the measurement process, an optical microscope lens and a charge-coupled device (CCD) camera system were used to record the related images. The whole force measurement process was performed under water. The peak data recorded in the force−distance curve was taken as the maximum adhesion force.

Materials. Na^+-Montmorillonite (MTM) was purchased from Southern Clay Products (Gonzales, TX). MTM (0.5 wt %) was vigorous stirred for 7 days prior to use. (3-Aminopropyl) triethoxysilane, poly(4-styrenesulfonic acid) solution (PSS, typical M_w: 70 000) and poly(diallyldimethylammonium chloride), (PDDA, typical M_w: 400 000−500 000) were purchased from Sigma-Aldrich. All other reagents and solvents were of analytical reagent grade and obtained from Sinopharm Chemical Reagent Co. Ltd., China. They were used without further purification. All solutions were prepared with ultrapure water (Milli-Q, 18.2 MΩ·cm). Artificial seawater was prepared by dissolving 2.6726 g of NaCl, 0.226 g of $MgCl_2$, 0.3248 g of $MgSO_4$, and 0.1153 g of $CaCl_2$ into 100 mL of Milli-Q water.

Conflict of Interest: The authors declare no competing financial interest.

Supporting Information Available: AFM phase image of MTM/PDDA bilayer; UV−vis absorbance spectra for deposition on a quartz slide monitored after every bilayer (MTM+PDDA) for the first 10 bilayers; XPS result of the $(MTM/PDDA)_{100\text{-salt}}$ film; the OCA and adhesive force measurements on $(MTM/PDDA)_{100}$ film; the oil contact angles and underwater adhesive forces between $(MTM/PDDA)_{100}$ film and oil with different surface tensions; AFM images and cross section analysis of $(MTM/PDDA)_{100}$ and $(MTM/PDDA)_{100\text{-salt}}$ films. This material is available free of charge *via* the Internet at http://pubs.acs.org.

Acknowledgment. The work was supported by National Natural Science Foundation of China (NSFC Grant No. 21103009, 2012CB933800, 21175140, 21171019), Beijing Natural Science Foundation (Grant No. 2122038), and the Key Research Program of the Chinese Academy of Sciences (Grant No. KJZD-EW-M01), the Fundamental Research Funds for the Central Universities, NCET-11-0584 and the Chinese 1000 Elites program and USTB start-up fund.

REFERENCES AND NOTES

1. Tuteja, A.; Choi, W.; Ma, M.; Mabry, J. M.; Mazzella, S. A.; Rutledge, G. C.; McKinley, G. H.; Cohen, R. E. Designing Superoleophobic Surfaces. *Science* **2007**, *318*, 1618–1622.
2. Liu, X.; Gao, J.; Xue, Z.; Chen, L.; Lin, L.; Jiang, L.; Wang, S. T. Bioinspired Oil Strider Floating at the Oil/Water Interface Supported by Huge Superoleophobic Force. *ACS Nano* **2012**, *6*, 5614–5620.
3. Liu, M.; Xue, Z.; Liu, H.; Jiang, L. Surface Wetting in Liquid−Liquid−Solid Triphase Systems: Solid-Phase-Independent Transition at the Liquid−Liquid Interface by Lewis Acid−Base Interactions. *Angew. Chem., Int. Ed.* **2012**, *51*, 8348–8351.
4. Cheng, Q.; Li, M.; Zheng, Y.; Su, B.; Wang, S. T.; Jiang, L. Janus Interface Materials: Superhydrophobic Air/Solid Interface and Superoleophobic Water/Solid Interface Inspired by a Lotus Leaf. *Soft Matter* **2011**, *7*, 5948–5951.
5. Jung, Y. C.; Bhushan, B. Wetting Behavior of Water and Oil Droplets in Three-Phase Interfaces for Hydrophobicity/Philicity and Oleophobicity/Philicity. *Langmuir* **2009**, *25*, 14165–14173.
6. Joly, L.; Biben, T. Wetting and Friction on Superoleophobic Surfaces. *Soft Matter* **2009**, 2549–2557.
7. Tuteja, A.; Choi, W.; McKinley, G. H.; Cohen, R. E.; Rubner, M. F. Design Parameters for Superhydrophobicity and Superoleophobicity. *MRS Bull.* **2008**, *33*, 752–758.
8. Choi, W.; Tuteja, A.; Mabry, J. M.; Cohen, R. E.; McKinley, G. H. A Modified Cassie−Baxter Relationship to Explain Contact Angle Hysteresis and Anisotropy on Non-Wetting Textured Surfaces. *J. Colloid Interface Sci.* **2009**, *339*, 208–216.
9. Pan, S.; Kota, A. K.; Mabry, J. M.; Tuteja, A. Superomniphobic Surfaces for Effective Chemical Shielding. *J. Am. Chem. Soc.* **2012**, *135*, 578–581.
10. Kota, A. K.; Kwon, G.; Choi, W.; Mabry, J. M.; Tuteja, A. Hygro-Responsive Membranes for Effective Oil−Water Separation. *Nat. Commun.* **2012**, *3*, 1025.
11. Kota, A. K.; Li, Y.; Mabry, J. M.; Tuteja, A. Hierarchically Structured Superoleophobic Surfaces with Ultralow Contact Angle Hysteresis. *Adv. Mater.* **2012**, *24*, 5838–5843.
12. Srinivasan, S.; Chhatre, S. S.; Mabry, J. M.; Cohen, R. E.; McKinley, G. H. Solution Spraying of Poly(Methyl Methacrylate) Blends to Fabricate Microtextured, Superoleophobic Surfaces. *Polymer* **2011**, *52*, 3209–3218.
13. Wong, T.-S.; Kang, S. H.; Tang, S. K. Y.; Smythe, E. J.; Hatton, B. D.; Grinthal, A.; Aizenberg, J. Bioinspired Self-Repairing Slippery Surfaces with Pressure-Stable Omniphobicity. *Nature* **2011**, *477*, 443–447.
14. Takahashi, M.; Figus, C.; Malfatti, L.; Tokuda, Y.; Yamamoto, K.; Yoko, T.; Kitanaga, T.; Tokudome, Y.; Innocenzi, P. Strain-Driven Self-Rolling of Hybrid Organic-Inorganic Microrolls: Interfaces with Self-Assembled Particles. *NPG Asia Mater.* **2012**, *4*, e22.
15. Zhang, L.; Zhang, Z.; Wang, P. Smart Surfaces with Switchable Superoleophilicity and Superoleophobicity in Aqueous Media: Toward Controllable Oil/Water Separation. *NPG Asia Mater.* **2012**, *4*, e8.
16. Hejazi, V.; Nyong, A. E.; Rohatgi, P. K.; Nosonovsky, M. Wetting Transitions in Underwater Oleophobic Surface of Brass. *Adv. Mater.* **2012**, *24*, 5963–5966.
17. Yao, X.; Gao, J.; Song, Y.; Jiang, L. Superoleophobic Surfaces with Controllable Oil Adhesion and Their Application in Oil Transportation. *Adv. Funct. Mater.* **2011**, *21*, 4270–4276.
18. Wu, D.; Wu, S.; Chen, Q. D.; Zhao, S.; Zhang, H.; Jiao, J.; Piersol, J. A.; Wang, J. N.; Sun, H. B.; Jiang, L. Facile Creation of Hierarchical Pdms Microstructures with Extreme Underwater Superoleophobicity for Anti-Oil Application in Microfluidic Channels. *Lab Chip* **2011**, *11*, 3873–3879.
19. Campos, R.; Guenthner, A. J.; Meuler, A. J.; Tuteja, A.; Cohen, R. E.; McKinley, G. H.; Haddad, T. S.; Mabry, J. M. Superoleophobic Surfaces through Control of Sprayed-on Stochastic Topography. *Langmuir* **2012**, *28*, 9834–9841.
20. Yang, J.; Zhang, Z.-Z.; Men, X.-H.; Xu, X.-H. Superoleophobicity of a Material Made from Fluorinated Titania Nanoparticles. *J. Dispersion Sci. Technol.* **2011**, *32*, 485–489.
21. Yang, J.; Zhang, Z.; Men, X.; Xu, X.; Zhu, X. A Simple Approach to Fabricate Superoleophobic Coatings. *New J. Chem.* **2011**, *35*, 576–580.
22. Zhang, J.; Seeger, S. Superoleophobic Coatings with Ultralow Sliding Angles Based on Silicone Nanofilaments. *Angew. Chem., Int. Ed.* **2011**, *50*, 6652–6656.
23. Wang, H.; Xue, Y.; Ding, J.; Feng, L.; Wang, X.; Lin, T. Durable, Self-Healing Superhydrophobic and Superoleophobic Surfaces from Fluorinated-Decyl Polyhedral Oligomeric Silsesquioxane and Hydrolyzed Fluorinated Alkyl Silane. *Angew. Chem., Int. Ed.* **2011**, *50*, 11433–11436.
24. Cheng, Q.; Li, M.; Yang, F.; Liu, M.; Li, L.; Wang, S.; Jiang, L. An Underwater PH-Responsive Superoleophobic Surface with Reversibly Switchable Oil-Adhesion. *Soft Matter* **2012**, *8*, 2740–2743.
25. Liu, M.; Wang, S. T.; Wei, Z.; Song, Y.; Jiang, L. Bioinspired Design of a Superoleophobic and Low Adhesive Water/Solid Interface. *Adv. Mater.* **2009**, *21*, 665–669.
26. Liu, M.; Nie, F.-Q.; Wei, Z.; Song, Y.; Jiang, L. *In Situ* Electrochemical Switching of Wetting State of Oil Droplet on Conducting Polymer Films. *Langmuir* **2010**, *26*, 3993–3997.

27. Chen, L.; Liu, M.; Lin, L.; Zhang, T.; Ma, J.; Song, Y.; Jiang, L. Thermal-Responsive Hydrogel Surface: Tunable Wettability and Adhesion to Oil at the Water/Solid Interface. *Soft Matter* **2010**, *6*, 2708–2712.
28. Liu, X.; Zhou, J.; Xue, Z.; Gao, J.; Meng, J.; Wang, S. T.; Jiang, L. Clam's Shell Inspired High-Energy Inorganic Coatings with Underwater Low Adhesive Superoleophobicity. *Adv. Mater.* **2012**, *24*, 3401–3405.
29. Xu, L.-P.; Zhao, J.; Su, B.; Liu, X.; Peng, J.; Liu, Y.; Liu, H.; Yang, G.; Jlang, L.; Wen, Y.; Zhang, X.; Wang, S. T. An Ion-Induced Low-Oi-Adhesion Organic/Inorganic Hybrid Film for Stable Superoleophobicity in Seawater. *Adv. Mater.* **2013**, *25*, 606–611.
30. Tuteja, A.; Choi, W.; Mabry, J. M.; McKinley, G. H.; Cohen, R. E. Robust Omniphobic Surfaces. *Proc. Natl. Acad. Sci* . **2008**, *105*, 18200–18205.
31. Neves, N.; Mano, J. Structure/Mechanical Behavior Relationships in Crossed-Lamellar Sea Shells. *Mater. Sci. Eng., C* **2005**, *25*, 113–118.
32. Tang, Z.; Kotov, N. A.; Magonov, S.; Ozturk, B. Nanostructured Artificial Nacre. *Nat. Mater.* **2003**, *2*, 413–418.
33. Li, X. Q.; Zeng, H. C. Calcium Carbonate Nanotablets: Bridging Artificial to Natural Nacre. *Adv. Mater.* **2012**, *24*, 6277–6282.
34. Finnemore, A.; Cunha, P.; Shean, T.; Vignolini, S.; Guldin, S.; Oyen, M.; Steiner, U. Biomimetic Layer-by-Layer Assembly of Artificial Nacre. *Nat. Commun.* **2012**, *3*, 966.
35. Yao, H.-B.; Mao, L.-B.; Yan, Y.-X.; Cong, H.-P.; Lei, X.; Yu, S.-H. Gold Nanoparticle Functionalized Artificial Nacre: Facile *in Situ* Growth of Nanoparticles on Montmorillonite Nanosheets, Self-Assembly, and Their Multiple Properties. *ACS Nano* **2012**, *6*, 8250–8260.
36. Espinosa, H. D.; Juster, A. L.; Latourte, F. J.; Loh, O. Y.; Gregoire, D.; Zavattieri, P. D. Tablet-Level Origin of Toughening in Abalone Shells and Translation to Synthetic Composite Materials. *Nat. Commun.* **2011**, *2*, 173.
37. Li, Y.-Q.; Yu, T.; Yang, T.-Y.; Zheng, L.-X.; Liao, K. Bio-Inspired Nacre-Like Composite Films Based on Graphene with Superior Mechanical, Electrical, and Biocompatible Properties. *Adv. Mater.* **2012**, *24*, 3426–3431.
38. Podsiadlo, P.; Liu, Z.; Paterson, D.; Messersmith, P. B.; Kotov, N. A. Fusion of Seashell Nacre and Marine Bioadhesive Analogs: High-Strength Nanocomposite by Layer-by-Layer Assembly of Clay and L-3,4-Dihydroxyphenylalanine Polymer. *Adv. Mater.* **2007**, *19*, 949–955.
39. Sun, J.; Bhushan, B. Hierarchical Structure and Mechanical Properties of Nacre: A Review. *RSC Adv.* **2012**, *2*, 7617–7632.
40. Walther, A.; Bjurhager, I.; Malho, J.-M.; Ruokolainen, J.; Berglund, L.; Ikkala, O. Supramolecular Control of Stiffness and Strength in Lightweight High-Performance Nacre-Mimetic Paper with Fire-Shielding Properties. *Angew. Chem., Int. Ed.* **2010**, *49*, 6448–6453.
41. Yao, H.-B.; Tan, Z.-H.; Fang, H.-Y.; Yu, S.-H. Artificial Nacre-Like Bionanocomposite Films from the Self-Assembly of Chitosan−Montmorillonite Hybrid Building Blocks. *Angew. Chem., Int. Ed.* **2010**, *49*, 10127–10131.
42. Podsiadlo, P.; Michel, M.; Critchley, K.; Srivastava, S.; Qin, M.; Lee, J. W.; Verploegen, E.; Hart, A. J.; Qi, Y.; Kotov, N. A. Diffusional Self-Organization in Exponential Layer-by-Layer Films with Micro- and Nanoscale Periodicity. *Angew. Chem., Int. Ed.* **2009**, *48*, 7073–7077.
43. Podsiadlo, P.; Kaushik, A. K.; Arruda, E. M.; Waas, A. M.; Shim, B. S.; Xu, J.; Nandivada, H.; Pumplin, B. G.; Lahann, J.; Ramamoorthy, A.; Kotov, N. A. Ultrastrong and Stiff Layered Polymer Nanocomposites. *Science* **2007**, *318*, 80–83.
44. Zhuk, A.; Mirza, R.; Sukhishvili, S. Multiresponsive Clay-Containing Layer-by-Layer Films. *ACS Nano* **2011**, *5*, 8790–8799.
45. Wang, J.; Lin, L.; Cheng, Q.; Jiang, L. A Strong Bio-Inspired Layered Pnipam−Clay Nanocomposite Hydrogel. *Angew. Chem., Int. Ed.* **2012**, *51*, 4676–4680.
46. Srivastava, S.; Kotov, N. A. Composite Layer-by-Layer (LBL) Assembly with Inorganic Nanoparticles and Nanowires. *Acc. Chem. Res.* **2008**, *41*, 1831–1841.
47. Kovtyukhova, N. I.; Ollivier, P. J.; Martin, B. R.; Mallouk, T. E.; Chizhik, S. A.; Buzaneva, E. V.; Gorchinskiy, A. D. Layer-by-Layer Assembly of Ultrathin Composite Films from Micron-Sized Graphite Oxide Sheets and Polycations. *Chem. Mater.* **1999**, *11*, 771–778.
48. Tang, Z.; Wang, Y.; Podsiadlo, P.; Kotov, N. A. Biomedical Applications of Layer-by-Layer Assembly: From Biomimetics to Tissue Engineering. *Adv. Mater.* **2006**, *18*, 3203–3224.
49. Keller, S. W.; Kim, H. N.; Mallouk, T. E. Layer-by-Layer Assembly of Intercaltion Compounds and Heterostructures on Surfaces: Toward Molecular "Beaker" Epitaxy. *J. Am. Chem. Soc.* **1994**, *116*, 8817–8818.
50. Lide, D. R. *CRC Handbook of Chemistry and Physics*, 90th ed.; CRC Press: Boca Raton, FL, 2009.
51. Harvey, E. H. The Surface Tension of Crude Oils. *Ind. Eng. Chem.* **1925**, *17*, 85.
52. http://www.etc-cte.ec.gc.ca/databases/Oilproperties/pdf/WEB_Petroleum_Ether.pdf.
53. Jin, T.; Jiyu, S.; Jiang, Z. Nanoindentation of Biomaterials. In *Handbook of Nanophysics*; CRC Press: Boca Raton, FL, 2010; pp 1−16.
54. Briscoe, B.; Fiori, L.; Pelillo, E. Nano-Indentation of Polymeric Surfaces. *J. Phys. D: Appl. Phys.* **1999**, *31*, 2395–2405.
55. Gao, C.; Donath, E.; Moya, S.; Dudnik, V.; Möhwald, H. Elasticity of Hollow Polyelectrolyte Capsules Prepared by the Layer-by-Layer Technique. *Eur. Phys. J. E* **2001**, *5*, 21–27.
56. Podsiadlo, P.; Kaushik, A. K.; Shim, B. S.; Agarwal, A.; Tang, Z.; Waas, A. M.; Arruda, E. M.; Kotov, N. A. Can Nature's Design Be Improved Upon? High Strength, Transparent Nacre-Like Nanocomposites with Double Network of Sacrificial Cross Links. *J. Phys. Chem. B* **2008**, *112*, 14359–14363.
57. Dodoo, S.; Steitz, R.; Laschewsky, A.; von Klitzing, R. Effect of Ionic Strength and Type of Ions on the Structure of Water Swollen Polyelectrolyte Multilayers. *Phys. Chem. Chem. Phys.* **2011**, *13*, 10318–10325.
58. Dubas, S. T.; Schlenoff, J. B. Factors Controlling the Growth of Polyelectrolyte Multilayers. *Macromolecules* **1999**, *32*, 8153–8160.
59. Gong, X.; Gao, C. Influence of Salt on Assembly and Compression of PDADMAC/PSSMA Polyelectrolyte Multilayers. *Phys. Chem. Chem. Phys.* **2009**, *11*, 11577–11586.